

Maximum Entropy for Gravitational Wave Data Analysis: Inferring the Physical Parameters of Core-Collapse Supernovae

T. Z. Summerscales¹

Center for Gravitational Wave Physics, Penn State University, University Park, PA 16802

`tzs@gravity.psu.edu`

Adam Burrows

Steward Observatory, University of Arizona, 933 North Cherry Avenue, Tucson, AZ 85721

`burrows@zenith.as.arizona.edu`

Christian D. Ott

*Max-Planck-Institut für Gravitationsphysik, Albert-Einstein-Institut, Am Mühlenberg 1,
14476 Golm/Potsdam, Germany*

`cott@aei.mpg.de`

and

Lee Samuel Finn

Center for Gravitational Wave Physics, Penn State University, University Park, PA 16802

`lsfinn@psu.edu`

ABSTRACT

The gravitational wave signal arising from the collapsing iron core of a Type II supernova progenitor star carries with it the imprint of the progenitor's mass, rotation rate, degree of differential rotation, and the bounce depth. Here, we show how to infer the gravitational radiation waveform of a core collapse event from noisy observations in a network of two or more LIGO-like gravitational wave detectors and, from the recovered signal, constrain these source properties. Using these techniques, predictions from recent core collapse modeling efforts, and the

¹Now at Department of Physics, Andrews University, Berrien Springs, MI, 49104

LIGO performance during its S4 science run, we also show that gravitational wave observations by LIGO might have been sufficient to provide reasonable estimates of the progenitor mass, angular momentum and differential angular momentum, and depth of the core at bounce, for a rotating core collapse event at a distance of a few kpc.

Subject headings: gravitational waves — methods: data analysis — supernovae: general

1. INTRODUCTION

The gravitational waves that we expect to observe in large detectors such as LIGO (Waldman & the LIGO Science Collaboratio 2006; Mandic 2006), Virgo (Acernese et al. 2006), GEO600 (Lück et al. 2006), TAMA300 (Takahashi & the TAMA Collaboration 2004) and LISA (Robertson 2000; Rüdiger 2004), reflect the coherent evolution of the most compact part of the source mass distribution. From the observed waves we have the potential to infer the factors that govern that evolution. For example, the evolution of the collapsing stellar core in a type II supernova is determined in part by the progenitor mass density and angular momentum distributions in the inner core. None of these properties of the progenitor can be directly determined from the electromagnetic radiation we observe when the shock emerges from the stellar envelope. In addition, the forces that govern the evolution of the core depend upon many things that are unknown, or poorly modeled, today (for example, the matter equation of state, the role played by neutrinos and neutrino radiation transport, general relativity, convection and non-axisymmetry). The gravitational waves emitted during the collapse phase and its aftermath carry the signature of all these preconditions and the dynamics that govern both the collapse and subsequent rebound. Reading that signature requires inferring the waveform from the noisy detector observations. Here, we develop a new method for inferring the gravitational radiation waveform from the noisy data from two or more detectors, based on Jaynes’ principle of maximum entropy (Jaynes 1957a,b), demonstrate its effectiveness when applied to the discovery of signals arising from simulated rotating iron core collapse buried in simulated detector noise, and show how the inferred waveform can be used, in principle, to gain insight into the properties of the source.

The first problem addressed in this study is the problem of inferring the gravitational wave signal from the data produced by the detectors, also referred to as the deconvolution or inverse problem. Inverse problems generally have been long-recognized as a problem to be approached with great care (see Evans & Stark (2002) for a recent review). The detector response, which relates the incident gravitational wave to the signal observed in the detector,

is generally an ill-conditioned function; additionally, the presence of additive noise generally confuses the observation. Together, the noise and the ill-conditioned detector response generally thwart naïve attempts at signal deconvolution. Early attempts at gravitational wave signal deconvolution explored a least-squares or maximum likelihood approach to deconvolution: e.g., Gürsel & Tinto (1989) developed a procedure for inferring a plane wave signal incident on a network of detectors with a frequency-independent response, in which case the problem response is well-conditioned. These techniques tend to over-fit the observations; additionally, realistic detectors have frequency responses that are ill-conditioned and this complicates a least-squares or maximum likelihood approach to deconvolution. More recent efforts have explored regularized methods for inferring the incident gravitational radiation waveform (Rakhmanov 2006). Here, we use the *maximum entropy* principle to regularize the deconvolution problem, developing an application to the gravitational wave inference problem that is applicable in the general case of a frequency dependent and ill-conditioned detector response and avoids over-fitting the observations in the presence of additive detector noise. Going beyond the problem of inferring the incident wave, we use the inferred waveform to explore how, and how well gravitational wave observations of this kind can be used to learn about the source.

Maximum entropy approaches to deconvolution have a long heritage in astronomical image reconstruction (Ponsonby 1973; Gull & Daniell 1978, 1979; Skilling & Bryan 1984; Steenstrup 1985; Shevgaonkar 1987; Nityananda & Narayan 1982, 1983; Narayan & Nityananda 1986; Pantin & Starck 1996; Starck & Pantin 1996, 1997; Barreiro et al. 2001; Maisinger et al. 2004), where they have been used in all wavebands. Recent examples of the use of maximum entropy based methods include the reconstruction of the cosmic microwave background (Maisinger et al. 1997; Vielva et al. 2001) including maps based on data from WMAP (Bennett et al. 2003) and COBE (Jones et al. 1998, 1999; Barreiro et al. 2004). Our work applies that heritage to the simpler problem of reconstructing the time-dependent plane wave signal incident on a network of gravitational wave detectors from their time series response.

Once we have inferred the incident signal, we are faced with a second problem of inference: identifying the properties of the source from the signal. One way of associating gravitational waveforms with supernova properties is to compare the inferred waveform with models arising from simulations that explore the signal dependency over a broad range of physical parameters. We should expect the inferred waveform to have the most in common with the simulated waveforms arising from models whose character is most similar to the actual source. Here, we compare, using the cross-correlation, inferred waveforms with simulated waveforms arising from different rotating core collapse models, assuming that models whose signal shows the greatest correlation are the ones most likely to be similar to the

source.¹

Section 2 describes the application of maximum entropy method that we have developed to infer the time-dependent gravitational wave signal incident on a network of detectors. In § 3 we demonstrate the effectiveness of the maximum entropy method in inferring a signal waveform buried in noisy data. Section 4 reviews the expected gravitational-wave emission processes in core-collapse supernovae and describes the recently produced catalog of rotating core-collapse waveforms by Ott et al. (2004) and the physics that went into the considered models. We use these simulated core-collapse signals to characterize how well our procedure for inferring the incident signal and characterizing the source works. Finally, in § 5 we summarize our conclusions and directions for further study.

One important goal with this paper is to connect the two communities of gravitational wave experimentalists and supernova modelers in a way that has not been done in the past. Future gravitational wave models can be put through the pipeline established with this paper so that we can obtain more credible estimates of what might be possible with either initial or advanced LIGO, Virgo, GEO600, or TAMA300, or with any combination of these, for any theoretical model. This has simply never been done for any collapse models, and is a novelty of this paper that we hope will stimulate further interactions between astrophysicists doing supernova simulations and the gravitational wave detection and data-analysis communities.

2. Maximum Entropy Signal Deconvolution

Focus attention on the observed response \mathbf{d} of a network of detectors to a plane-fronted gravitational wave burst \mathbf{h} incident on the network from a known direction. The observation \mathbf{d} is a collection of noisy time series. Each noisy time series corresponds to a different detector’s response to the incident burst. Symbolically we may write

$$\mathbf{d} = \mathbf{R} * \mathbf{h} + \mathbf{n} \tag{1}$$

where $\mathbf{R} * \mathbf{h}$ is the convolution of the detector network response \mathbf{R} with the incident gravitational wave burst \mathbf{h} , and \mathbf{n} represents the measurement noise associated with the detectors in the network. Our goal is to infer \mathbf{h} given the observation \mathbf{d} and our knowledge of the network response \mathbf{R} and the statistical properties of the network’s noise \mathbf{n} .

¹Note the distinction between correlation and the more involved matched filtering (Finn 1992; Finn & Chernoff 1993). Matched filtering is a useful analysis technique when the functional form of the signal being sought is known precisely. Here, we presume that we have only a qualitative model of the signal dependence on the physical parameters of interest. In that case, using the full apparatus of matched filtering could very well lead us to reject real signals because the match to the model is only qualitative.

In realistic problems the network response \mathbf{R} is ill-conditioned: i.e., it does not have an inverse, the inverse is not unique, or the solution \mathbf{x} to an equation of the form $\mathbf{R} * \mathbf{x} = \mathbf{b}$ is sensitive to small perturbations to \mathbf{b} . For example, the detector network may be insensitive to gravitational wave power in some frequency bands, or to signals propagating in some particular directions, or unable to distinguish between the two gravitational wave polarization states, etc. Even in those cases where the response is invertible and well-conditioned, applying the inverse to \mathbf{d} does not distinguish between the signal \mathbf{h} and the noise \mathbf{n} . In cases like these, additional assumptions about the solution must \mathbf{h} must be introduced in order to find a stable and physically meaningful solution.

Framing the problem of deconvolution in the language of Bayesian inference provides guidance on how to proceed in determining \mathbf{h} . Let \mathbf{h}' be a conjecture for the incident wave. In a Bayesian approach to the problem of inference we seek

$$f(\mathbf{h}'|\mathbf{d}, \mathbf{R}, \mathbf{N}, \mathcal{I}) = \left(\begin{array}{l} \text{the probability density that } \mathbf{h}' \text{ is the incident wave given the} \\ \text{data } \mathbf{d}, \text{ the detector response } R, \text{ the noise characterization} \\ \mathbf{N}, \text{ and other unenumerated assumptions } \mathcal{I}. \end{array} \right). \quad (2a)$$

A good point estimate of the incident radiation is the \mathbf{h}' that maximizes $f(\mathbf{h}'|\mathbf{d}, \mathbf{R}, \mathbf{N}, \mathcal{I})$.

Following Bayes Law, the probability distribution f may be “factored” into the product of two other distributions:

$$f(\mathbf{h}'|\mathbf{d}, \mathbf{R}, \mathbf{N}, \mathcal{I}) \propto g(\mathbf{d}|\mathbf{h}', \mathbf{R}, \mathbf{N}, \mathcal{I})q(\mathbf{h}'|\mathcal{I}), \quad (3a)$$

where

$$g(\mathbf{d}|\mathbf{h}', \mathbf{R}, \mathbf{N}, \mathcal{I}) = \left(\text{likelihood function for } \mathbf{d} \text{ given } \mathbf{h}' \right) \quad (3b)$$

$$q(\mathbf{h}'|\mathcal{I}) = \left(a \text{ priori expectations regarding the incident wave.} \right) \quad (3c)$$

Focus attention first on the likelihood function $g(\mathbf{h}'|\mathcal{I})$. The most common characterization \mathbf{N} of the noise statistical properties is its mean and covariance (or, equivalently, its power- and cross-spectral density). Let \mathbf{N} denote the noise correlation function and assume, without loss of generality, that noise mean vanishes. In that case the likelihood function may be written

$$\log g(\mathbf{d}|\mathbf{h}', \mathbf{R}, \mathbf{N}, \mathcal{I}) = -\frac{1}{2}\chi^2(\mathbf{d}, \mathbf{h}', \mathbf{R}, \mathbf{N}) + \text{const.} \quad (4)$$

where

$$\chi^2(\mathbf{d}, \mathbf{h}', \mathbf{R}, \mathbf{N}) = (\mathbf{d} - \mathbf{R} * \mathbf{h}')^T * \mathbf{N}^{-1} * (\mathbf{d} - \mathbf{R} * \mathbf{h}') \quad (5)$$

which may be evaluated directly: i.e., without inverting the generally ill-conditioned response \mathbf{R} .

When the observables \mathbf{d} over-determine the incident wave \mathbf{h} , it is tempting to ignore $q(\mathbf{h}'|\mathcal{I})$ in equation 3, minimize χ^2 (i.e., maximize the likelihood) over \mathbf{h}' , and declare that \mathbf{h}' is the inferred incident wave. This is, with minor variation, the approach taken by Gürsel & Tinto (1989). While an entirely legitimate approach to deconvolution, maximum likelihood methods generally over-fit \mathbf{d} : i.e., they find a \mathbf{h}' that leaves a residual $\mathbf{d} - \mathbf{R} * \mathbf{h}'$ that is inconsistent with the known noise properties \mathbf{N} . One role played by $q(\mathbf{h}'|\mathcal{I})$ is to resist this tendency toward over-fitting the noisy data.

In general, $q(\mathbf{h}'|\mathcal{I})$, which represents the general credibility that we give to different \mathbf{h}' before we ask what can be learned from the observations \mathbf{d} , may derive from previous observation, source modeling or other theoretical investigation, or other considerations. In the problem we address here, we are interested in inferring the form of a gravitational wave burst absent previous observations, detailed simulations or theoretical modeling to guide the choice of $q(\mathbf{h}'|\mathcal{I})$. In the absence of this kind of guidance we ask for a q that, in some meaningful sense, corresponds to a minimum of informative content. Information theory provides a meaningful sense for the information content of a distribution like q . The negative of that content is referred to *information entropy* and the distribution q that maximizes this entropy and is consistent with our other assumptions \mathcal{I} is the maximum entropy distribution, or the *entropic prior*.

To find the form of the entropic prior $q(\mathbf{h}'|\mathcal{I})$, first focus on the general considerations that we can bring to bear on the properties of a general burst \mathbf{h}' . Writing \mathbf{h}' as the sum of two time series, corresponding to the two polarizations \mathbf{h}'_+ and \mathbf{h}'_\times of an incident gravitational wave, we note that

- Lacking any reason to presume that the source is oriented in a particular way relative to the line-of-sight to the detector, the prior should be invariant under an arbitrary rotation of $+$ into \times polarization;
- Lacking any reason to presume that the gravitational wave burst arrives at a particular moment in time, the prior should be time independent;
- We should assume no particular smoothness or correlation in \mathbf{h}' over time (i.e., assume nothing about burst power a function of frequency); and, finally,
- We should assume that $-\mathbf{h}'_+$ is as probable as \mathbf{h}'_+ (and similarly for $\pm\mathbf{h}'_\times$).

Under these general invariance conditions, Hobson & Lasenby (1998) found the entropic

prior that should apply to \mathbf{h} , whose values can equally well be positive or negative, to have the form

$$q(\mathbf{h}|m, \alpha, \mathcal{I}) \propto \exp[\alpha S(\mathbf{h}, m)] \quad (6a)$$

where

$$S(\mathbf{h}, m) = \sum_i [s(h_{+,i}, m) + s(h_{\times,i}, m)] \quad (6b)$$

$$s(x, m) = \Psi(x, m) - 2m - x \log \frac{\Psi + x}{2m}, \quad (6c)$$

$$\Psi = (x^2 + 4m^2)^{1/2}, \quad (6d)$$

m is a to-be-determined constant that sets the scale on \mathbf{h} , and α is another to-be-determined constant related to the dimension of \mathbf{h} (i.e., the number of samples of h_+ and h_\times that we are inferring), and $h_{+,i}$ and $h_{\times,i}$ are the individual samples of \mathbf{h}_+ and \mathbf{h}_\times .

Setting aside for the moment the assignment of m and α , the entropic prior $q(\mathbf{h}|m, \alpha, \mathcal{I})$ leads us to choose as the best estimate of \mathbf{h} the \mathbf{h}' that minimizes

$$F(\mathbf{h}'|\mathbf{d}, \mathbf{N}, \alpha, m) = \frac{1}{2}\chi^2(\mathbf{h}, \mathbf{R}, \mathbf{N}, \mathbf{d}) - \alpha S(\mathbf{h}, m). \quad (7)$$

Stripped of its Bayesian statistical motivation, we recognize that maximum entropy deconvolution amounts to the solution of the inverse problem via regularization with a specific choice for the regularization function ($\alpha S(\mathbf{h}, m)$).

It remains to determine α and m . Clearly, different choices of α and m will lead to different \mathbf{h} minimizing $F(\mathbf{h}|\mathbf{d}, \mathbf{N}, \alpha, m)$. Too small an α will lead to over-fitting of the noisy data (i.e., less weight on the prior) and too large an α will lead to a solution \mathbf{h} that approaches 0 (i.e., the \mathbf{h} that maximizes the entropy functional $S(\mathbf{h}, m)$). Similarly, if m is large then m^2 and α become degenerate: i.e., changing m and α such that $m^2\alpha$ is constant leaves the posterior unchanged.

In the end, of course, the probability distribution f should not depend on either α or m . Gull (1989) (see also Mackay 1992) showed how, in the limit that $s(h|m) \sim (h/m)^2$, α should be chosen such that

$$\max_{\mathbf{h}'} F(\mathbf{h}'|\mathbf{d}, \mathbf{N}, \alpha, m) = N/2, \quad (8)$$

where N is the number of data samples in the observation \mathbf{d} , and we adopt that approximation here.

We make the the choice of m in a different way. Using Bayes' Law, we write the posterior probability density of m given the observations \mathbf{d} as

$$r(m|\mathbf{d}, \mathbf{R}, \mathbf{N}, \alpha, \mathcal{I}) = \int D\mathbf{h} f(\mathbf{h}|\mathbf{d}, \mathbf{R}, \mathbf{N}, \alpha, m, \mathcal{I})u(m|\mathcal{I}), \quad (9)$$

where u is the prior on m . We choose for m the one that maximizes r .

To find this m , we assume that f is sufficiently sharply peaked in m that the dependence of r on u is unimportant, in which case we can take u to be constant. Recalling that

$$g(\mathbf{d}|\mathbf{h}, \mathbf{R}, \mathbf{N}, \mathcal{I}) = Z_g^{-1} \exp\left(-\frac{1}{2}\chi^2\right) \quad (10a)$$

$$q(\mathbf{h}'|\mathcal{I}) = Z_q^{-1} \exp(\alpha S) \quad (10b)$$

where

$$Z_g = \int D\mathbf{d} \exp\left(-\frac{1}{2}\chi^2\right) \quad (10c)$$

$$Z_q = \int D\mathbf{h} \exp(\alpha S), \quad (10d)$$

we conclude that the most probable m is the m' that maximizes

$$r(m|\mathbf{d}, \mathcal{I}) = \frac{Z_f}{Z_g Z_q}, \quad (11a)$$

where

$$Z_f = \int D\mathbf{h} \exp\left(-\frac{1}{2}\chi^2 + \alpha S\right). \quad (12)$$

and Z_f and Z_q are both functions of m through dependence on S .

The integral Z_g is independent of m and \mathbf{d} and can be computed exactly (the integrand is a Gaussian):

$$\log Z_g = \frac{N_d}{2} \log(2\pi) + \frac{1}{2} \log \det \mathbf{N}, \quad (13)$$

where N_d is the number of elements of \mathbf{d} . In a general setting we can evaluate $\log \det \mathbf{N}$ by forming the Cholesky decomposition of \mathbf{N} , which is an upper triangular matrix \mathcal{N} such that \mathbf{N} is equal to $\mathcal{N}^T \mathcal{N}$; then,

$$\log \det \mathbf{N} = 2 \log \det \mathcal{N} = 2 \sum_{j=1}^{N_d} \log \mathcal{N}_{jj}, \quad (14)$$

where \mathcal{N}_{jj} is the j^{th} element on the main diagonal of \mathcal{N} .

The integrals Z_f and Z_q are not as simple as Z_g ; however, we can approximate Z_f and Z_q via the method of steepest descent. In the case of Z_f it is helpful to note that $(-1/2)\chi^2 + \alpha S$ is the negative of the functional F in equation 7, which we have already minimized to find the best estimate \mathbf{h}' of \mathbf{h} for a given α . Thus,

$$Z_f = \int D\mathbf{h} \exp \left[-F(\mathbf{h}') + \frac{1}{2}(\mathbf{h} - \mathbf{h}')^T \cdot H(-F)|_{\mathbf{h}'} \cdot (\mathbf{h} - \mathbf{h}') \right], \quad (15)$$

where $H(F)|_{\mathbf{h}'}$ is the Hessian of F with respect to \mathbf{h} , evaluated at $\mathbf{h} = \mathbf{h}'$. Performing the multivariate Gaussian integration we find

$$\log Z_f \approx -F(\mathbf{h}') + \frac{N_h}{2} \log(2\pi) - \frac{1}{2} \log \det ||H(F)|_{\mathbf{h}'}|| \quad (16)$$

where N_h is the number of elements of \mathbf{h} . To calculate $\log \det ||H(F)||$ we first write it in the form

$$||H(F)|| = \mathbf{U}^T \mathbf{A}(\mathbf{I} - \mathbf{D})\mathbf{A}\mathbf{U}, \quad (17)$$

where \mathbf{U} and \mathbf{A} are upper-triangular and diagonal matrices, respectively, \mathbf{I} is the identity matrix, and \mathbf{D} is a sparse matrix with eigenvalues in $(-1, 1)$. Then

$$\log \det ||H(F)|| = 2 \log \det (\mathbf{A}\mathbf{U}) + \log \det (\mathcal{I} - \mathbf{D}). \quad (18)$$

The contribution $\log \det (\mathbf{A}\mathbf{U})$ is just the sum of the log of the diagonal elements of \mathbf{A} and \mathbf{U} . The $\log \det(\mathbf{I} - \mathbf{D})$ can then be evaluated using the Monte Carlo methods introduced by Barry & Pace (1999).

A similar calculation allows us to evaluate Z_q : i.e.,

$$Z_q \approx \exp[\alpha S(\mathbf{h}_0)] (2\pi)^{N_h/2} (\det ||H(-\alpha S)|_{\mathbf{h}_0}||)^{-1/2}, \quad (19)$$

where $H(-\alpha S)|_{\mathbf{h}_0}$ is the Hessian of $-\alpha S$ with respect to \mathbf{h} , evaluated at the $\mathbf{h} = \mathbf{h}_0$ that maximizes $\alpha S(\mathbf{h})$. For our entropy functional $\mathbf{h}_0 = 0$ and

$$H(\alpha S)|_{\mathbf{h}_0} = \alpha/2m; \quad (20)$$

so

$$\log Z_q \approx \frac{N_h}{2} [\log(2\pi) - \log(\alpha/2m)]. \quad (21)$$

In the examples considered in section 4 the best estimate \mathbf{h}' remains approximately constant as m ranges over a few orders of magnitude near the value that maximizes $\log r(m|\mathbf{d}) = \log Z_f - \log Z_g - \log Z_q$ allowing us to conclude, post hoc, that the precise value of m is not important to our conclusions.

3. TESTING MAXIMUM ENTROPY USING SIMPLIFIED DETECTOR RESPONSES

Before studying our ability to infer a waveform from the response of the LIGO detector network, we test the effectiveness of the maximum entropy method on a simpler data set. For this simpler data set we take a model waveform drawn from Ott et al. (2004), a very simple model for the response of two “detectors” and use those to determine the signal content $\mathbf{R} * \mathbf{h}$ of simulated data \mathbf{d} . To the signal content we add white noise \mathbf{n} , taken to be independent between the two detectors. Given the response function and the statistical character of the noise, we infer, as described in the previous section, the incident wave, which we compare to the actual incident wave via cross-correlation.

For this simple test, we consider only two detectors and model the signal content of the observed data as the convolution of the incident signal \mathbf{h} with finite impulse response filters \mathbf{r}_1 and \mathbf{r}_2 :

$$d_{j,k}^h = \sum_{\ell=0} r_{j,\ell} h_{j,k-\ell} \quad (22a)$$

with

$$\mathbf{r}_1 = (1, -2, 2), \quad \text{and} \quad (22b)$$

$$\mathbf{r}_2 = (1, +2, 2). \quad (22c)$$

To the \mathbf{d}^h we add normally distributed white noise, whose amplitude we characterize by the mean signal-to-noise ratio ρ , defined by

$$\rho^2 = \frac{1}{2} (\rho_1^2 + \rho_2^2), \quad (23a)$$

$$\rho_k^2 = \sum_{j=0}^N \frac{(\mathbf{r}_k * \mathbf{h})^2}{N\sigma_k^2}, \quad (23b)$$

and with σ_k^2 equal to the detector k noise variance.² For \mathbf{h} we use the waveform model s15A1000B0.1 of Ott et al. (2004), which is further described in § 4.1 below.

From the simulated data we infer a waveform \mathbf{h}' and calculate the correlation of the

²It is important to note that the signal-to-noise as defined above relies on the unknown real signal; correspondingly, it is not the physical observable signal-to-noise. We use it here as the appropriate measure of the ratio of signal power to noise power in the *simulated* data, and to facilitate comparison with certain experimental results published by the LIGO Scientific Collaboration, which report signal-to-noise on an idealized waveform and not the actual observed data (see, for example Abbott et al. (2004)).

inferred and actual incident signal:

$$C(j) = \frac{\sum_k h_{k+j} h'_k}{|\mathbf{h}'| |\mathbf{h}|} \quad (24a)$$

where

$$|\mathbf{x}|^2 = \sum_k x_k^2. \quad (24b)$$

In Figure 1 we report the maximum of $C(j)$ over all lags j for a range of ρ^2 . For the simple example of this section, the maximum entropy method described here is able to recover greater than 70% of the power in the original signal for ρ^2 greater than 60. For comparison, the amplitude-squared signal to noise ρ^2 typically cited as being necessary for a detection is on order 64 or greater (Finn & Chernoff 1993). In figures 2 and 3 we show examples of the inferred \mathbf{h}' for low and high ρ^2 .

4. APPLICATION TO LIGO

How well can we hope to characterize the astrophysics of core-collapse supernovae from the gravitational wave signature we observe? The detailed astrophysics of core-collapse supernovae is uncertain, difficult to model, and involves large-scale convection and other stochastic processes. For all these reasons, it is more likely that we will infer the features of the gravitational wave burst associated with a supernova and then use that inferred signal to validate our models, than that we will “discover” the gravitational wave signal from a core-collapse supernova by using matched filtering to extract it from deep within a noisy data stream.

As a first step toward exploring how, and how well, we may be able to diagnose the conditions of the collapsing core from the gravitational waves it radiates we use the techniques, described in the previous two sections, to infer a simulated signal embedded in LIGO-like noise and evaluate the cross-correlation between the inferred signal and a wide range of signals calculated from the models of Ott et al. (2004). We do this for

- LIGO data drawn from the S1–S4 science runs, evaluating the maximum distance at which there is a significant correlation between the inferred and simulated signals (cf. sec. 4.2.1);
- Simulated signals with varying maximum central density (cf. sec. 4.2.2), evaluating our ability to evaluate the properties of the core-collapse;

- Simulated signals with varying progenitor mass, evaluating our ability to test the correlation between progenitor models and the configuration of the collapsing stellar core (cf. sec. 4.2.3);
- Simulated signals with varying angular momentum and differential angular velocity, allowing us to explore the role that differential rotation plays in core collapse (cf. sec. 4.2.4).

We find that, even when the simulated signal is so weak that the inferred signal appears very different, the inferred signal still has its greatest cross-correlation with the simulated signal. We conclude that the model whose signal has the maximum cross-correlation with the inferred signal is likely to provide a good indication of the physical properties of the source.

4.1. The Gravitational Wave Signature of Core-Collapse Supernovae: Description of Core-Collapse Models

Gravitational wave emission from core-collapse supernovae may arise from a multitude of processes, including rotating core collapse and core bounce (e.g., Fryer et al. 2002; Dimmelmeier et al. 2002; Ott et al. 2004; Dimmelmeier et al. 2007), postbounce convective overturn, anisotropic neutrino emission (Burrows & Hayes 1996; Müller et al. 2004; Ott et al. 2006), nonaxisymmetric rotational instabilities of the protoneutron star (Rampp et al. 1998; Ott et al. 2007; Shibata & Sekiguchi 2005), or from the recently proposed protoneutron star core g-mode oscillations (Burrows et al. 2006, 2007; Ott et al. 2006; Ferrari et al. 2003). In addition and in the context of the core-collapse supernova – gamma-ray burst connection (Woosley & Bloom 2006), late-time black hole formation in a failed or weak core-collapse supernova may accompany gravitational wave emission from quasi-normal ring-down modes of the newly-formed black hole.

Of all the above emission processes, rotating iron core collapse and bounce is the most extensively modeled and best quantitatively and qualitatively understood. For these reasons we limit our present study to an analysis of the rotating core collapse and bounce signature only and use example templates computed from a set of 2D axisymmetric Newtonian core collapse simulations by Ott et al. (2004) which focused on the dynamics of rotational collapse and bounce. These represent a class of signatures of core collapse and are good templates with which to exercise the signal extraction technology we have developed. This paper is the first to put theoretical models of the gravitational wave signals of core collapse and bounce through a realistic detector pipeline and to attempt to extract physical information using

sophisticated signal processing algorithms.

The astrophysics models involved stellar progenitors with various masses: 11, 15, 20, and $25M_{\odot}$ calculated in Woosley & Weaver (1995). The simulations neglected the effects of neutrinos, general relativity, and magnetic fields, but used the realistic, finite-temperature nuclear equation of state of Lattimer & Swesty (1991). A small number of simulations also investigated stellar progenitor models from Heger et al. (2000) and Heger et al. (2004), which were evolved to the onset of iron core collapse with an approximate treatment of rotation (Heger et al. 2000, 2004) and angular momentum redistribution by magnetic torques (Heger et al. 2004). The gravitational wave signature extraction was performed using the Newtonian quadrupole formalism (see e.g. Misner et al. 1973).

The effects of rotation were investigated in Ott et al. (2004). The initial rotation of the progenitor was controlled by two parameters: the rotation parameter β where

$$\beta = \frac{E_{\text{rot}}}{|E_{\text{grav}}|}, \quad (25)$$

and the differential rotation scale parameter A , which is the distance from the rotational axis at which the rotational velocity drops to half that at the center. A is defined as

$$\Omega(r) = \Omega_0 \left[1 + \left(\frac{r}{A} \right)^2 \right]^{-1}, \quad (26)$$

where r is the distance from the axis of rotation and $\Omega(r)$ is the angular frequency at r .

When the progenitor is rotating slowly and β is small (zero to a few tenths of a percent), the collapse is halted when the inner core reaches supranuclear densities. The core bounces rapidly and then quickly rings down. When the progenitor rotates more rapidly and β is larger, the core collapse is halted by centrifugal forces and the core bounces at subnuclear densities. The core then undergoes multiple damped, harmonic oscillator-like expansion-collapse-bounce cycles³ The initial degree of differential rotation affects the value of β at which this bounce type transition occurs. A progenitor with a smaller value of A experiences a greater amount of differential rotation and hence, a more rapidly rotating inner core. As a result, the transition from a supranuclear to a subnuclear bounce occurs for a lower value of β .

The models of Ott et al. (2004) yield absolute values of the dimensionless maximum gravitational wave strain h_{max} in the interval $2 \times 10^{-23} \leq h_{\text{max}} \leq 1.25 \times 10^{-20}$ at a detector

³Recent results of Ott et al. (2007) and Dimmelmeier et al. (2007) suggest that such multiple-bounce dynamics are less likely when general relativity and deleptonization are taken into account.

distance of 10 kpc. The total energy radiated (E_{GW}) lies in the range $1.4 \times 10^{-11} M_{\odot} c^2 \leq E_{\text{GW}} \leq 2.21 \times 10^{-8} M_{\odot} c^2$ and most of it is emitted in the primary gravitational wave burst associated with core bounce. The energy spectra peak in the frequency interval $20 \text{ Hz} \leq f_{\text{peak}} \leq 600 \text{ Hz}$ with rapid and differential rotators having peaks at low frequencies and moderate and rigid rotators peaking at high frequencies.

4.2. Gravitational wave observations of rotating stellar core collapse

In all the simulations described here we used Ott et al. (2004) model s15A1000B0.1 as the “real” signal, and correlated the inferred signal with other models in the Ott et al. (2004) catalog. Model s15A1000B0.1 corresponds to a $15 M_{\odot}$ Woosley & Weaver (1995) progenitor with rotation parameter β equal to 0.1% and differential rotation scale parameter A equal to 1000 km. We scaled this signal to represent core collapse events at different distances and projected the incident signal onto the LIGO 4-km Hanford WA (LHO) and Livingston, LA (LLO) detectors. For the purpose of this study we assumed that the core collapse was directly overhead of the LHO site. Since the Ott et al. (2004) core collapse models are axisymmetric the gravitational waves they emit are linearly polarized. We chose the polarization angle to maximize the response of the LHO detector. Finally, we used the actual response functions for the LHO and LLO detectors characteristic of LIGO’s S4 science run (González et al. 2004) and simulated the detector noise by adding white noise with power spectral density amplitude approximately equal to the noise amplitude at 100 Hz in the corresponding science run (Lazzarini 2005).⁴ Finally, we used the maximum entropy method described above to find the best point estimate of the embedded signal and cross-correlated this estimate signal with different signals drawn from the Ott et al. (2004) parameter survey. The subsections below describe our observations based on this study.

⁴At the frequencies where the signal power (in units of squared strain) of the simulated core collapse event gravitational wave signals peaks ($\sim 500 \text{ Hz}$) the noise power spectral density in any of the current generation of interferometric gravitational wave detectors is increasing relatively slowly with frequency. (Very little is known concerning the cross-correlation in the noise of two separated detectors, other than that it is very small.) While we have chosen to make this demonstration with white noise, the maximum entropy analysis method introduced above naturally accommodates any noise covariance: cf. the paragraph including equation (4).

4.2.1. *Science Run and Survey Range*

Before discussing how well we can distinguish between different core collapse models we looked at LIGO’s sensitivity, in its first four science runs (S1, S2, S3 and S4), to gravitational waves from rotating core collapse and how close a core collapse event would have needed to be in order that LIGO would have been able to infer its waveform with reasonable accuracy. For this purpose we used the detector response functions corresponding to the first four science runs (Adhikari et al. 2003; Adhikari et al. 2003; González et al. 2004) and simulated the detector noise by white noise with power spectral density amplitude approximately equal to the noise amplitude at 100 Hz in the corresponding science run (Lazzarini 2002, 2003, 2004, 2005).

Figure 4 shows the maximum cross-correlation, for each of the first four science runs, between the inferred and actual waveforms as a function of the core collapse distance. There is a steady improvement, from S1 to S4, in maximum entropy’s ability to recover signals at greater distances, corresponding to improving detector sensitivity: by S4, we are able to infer the gravitational waveform from core collapse events that occur as far as a few kpc away. The up-tick in cross-correlation at the 1 kpc mark in curve for S3 sensitivity is the result of a discontinuous change in the most probable waveform (i.e., a new extrema becoming the global maximum in the probability function.)

The investigations described in the following sections, which delve into the source information present in the inferred signal, use the response and noise characteristic of the LIGO S4 science run.

4.2.2. *Bounce Type*

We can classify the models of Ott et al. (2004) into those that bounce at supranuclear, subnuclear and transitional central densities. Figure 5 shows the maximum cross-correlation between the inferred waveform, the actual waveform (a supranuclear bounce type), and three other waveforms that each have, within their respective categories (supernuclear, subnuclear and transitional), the greatest cross-correlation with the inferred waveform. Figure 6 shows these four waveforms themselves, each with strain scaled to a distance of 10 kpc. It is clear that the inferred waveform has the most in common with that generated from a model with the same, supranuclear, bounce type and that, for S4 detector sensitivities, our ability to distinguish bounce type fails for core collapse events more than 2-3 kpc distant.

4.2.3. *Mass*

Figure 7 shows the cross-correlation between the inferred and actual waveforms associated with core collapse models that differ by progenitor mass, but share the same rotational parameters. Figure 8 shows the waveforms used for the cross-correlations. Again, for S4 sensitivities the inferred waveform most closely resembles the waveform from the model with the same mass at distances up to 2-3 kpc.

4.2.4. *Rotation*

Figure 9 shows the cross-correlation between the inferred waveform, the actual waveform, and the waveforms associated with a set of models that differ only by rotation parameter β , while figure 10 shows the cross-correlations for models that differ only by the differential rotation parameter A (cf. eq. 26). Figures 11 and 12 show the waveforms for the set of models whose cross-correlations are shown in figures 9 and 10. As expected, the cross-correlation decreases as the rotational parameters of the models depart from those associated with the actual waveform.

5. DISCUSSION/CONCLUSIONS

The gravitational waves that we expect to observe with detectors like LIGO, VIRGO, GEO, TAMA and LISA (Waldman & the LIGO Science Collaboratio 2006; Mandic 2006; Acernese et al. 2006; Lück et al. 2006; Takahashi & the TAMA Collaboration 2004; Robertson 2000; Rüdiger 2004), reflect the coherent evolution of the most compact part of the source mass distribution. From the observed waves we thus have the potential to infer the details of that evolution. To take advantage of this opportunity, however, we must be able to infer the waveform from the noisy detector data and compare the inferred waveform to models that represent the range of possibilities.

Here, we have described one such method for inferring the radiation incident on a network of detectors, based on the principle of maximum entropy (Jaynes 1957a,b), and showed how such a comparison might be made, using gravitational wave signatures calculated from the rotating core collapse models of Ott et al. (2004) as an example. We have found, in the context of this example, that at the signal-to-noise ratios expected to be used as a threshold for detection of core-collapse supernova burst events the methods described here infer the incident gravitational wave signal with enough fidelity to distinguish between models of different maximum central density, angular momentum, differential rotation, and

progenitor mass.

To make the comparison between the inferred and model waveforms we have used the maximum of the cross-correlation between the two, choosing the model whose maximum cross-correlation with the inferred waveform is the greatest. A Bayesian treatment that assigns odds to different models given the inferred waveform is a natural next step; however, we note that a Bayesian treatment would involve the exponential of the cross-correlation function (as opposed to the maximum cross-correlation) marginalized over the lag. When the cross-correlation is a sharply peaked function, this will be proportional to the exponential of the maximum of the cross-correlation among the different models. Thus, we conclude that the cross-correlation as we use it here is almost certainly likely to choose the same model as a more sophisticated Bayesian analysis, except in those cases where the waveforms of the different models are nearly indistinguishable.

While our example applications have been in terms of two interferometers, there is nothing in the description of the method that specifies the number of detectors and the application to three or more detectors is no different than for two detectors. The maximum entropy method described here could be applied simultaneously to data from LIGO, Virgo, GEO600, TAMA and the operating bar detectors. For the particular simulations described above, adding any one of these detectors would most likely not improve maximum entropy's estimate of the signal, since we have chosen the optimal sky location and source orientation for the LIGO Hanford Observatory site. For a source so positioned the strain amplitude in the LIGO Livingston detector is 89% of that for the LHO detectors, while for the GEO600 site detector it is 42%, 22% for TAMA300, and 1% for Virgo. On the other hand, the addition of these other detectors to a real network would increase the overall sensitivity across the sky, as a source optimally oriented for Virgo would, by reciprocity, be very poorly oriented for the LHO detectors.

Gravitational wave astronomy is not yet a reality. Nevertheless, with the detectors now operating and the enhancements currently underway, it is only a matter of time before we have observations of from these instruments, from which we can gain insight into astronomical phenomena that are otherwise hidden from our sight. Methods like those described here will allow us to move beyond gravitational wave detection and realize the promise of gravitational wave astronomy.

TZS and LSF gratefully acknowledge informative discussions with Graham Woan, Malik Rakhmanov, Nelson Christensen, and Soumya Mohanty. TZS and LSF were supported by NSF through grant PHY-00-99559 and the Center for Gravitational Wave Physics. LSF also acknowledges the support of NSF through award PHY-05-55615, NASA through award

NNG05GF71G, and the Penn State Center for Space Research Programs. AB acknowledges support for this work from the Scientific Discovery through Advanced Computing (SciDAC) program of the DOE, grant numbers DE-FC02-01ER41184 and DE-FC02-06ER41452 and from the NSF under grant number AST-0504947. CDO thanks the Albert-Einstein-Institut for providing CPU time on their Peyote Linux cluster. The Center for Gravitational Wave Physics is funded by the National Science Foundation via cooperative agreement PHY 01-14375.

REFERENCES

- Abbott, B., et al. 2004, *Phys. Rev. D*, 69, 122001
- Acernese, F. et al. 2006, *Class. Quantum Grav.*, 23, S635
- Adhikari, R., Fritshel, P., González, G., Landry, M., Matone, L., Radkins, H., Takamori, A., & O’Reilly, B. 2003, Calibration of the LIGO detectors for the first LIGO scientific run, Tech. Rep. T030097-00-D, Laser Interferometer Gravitational Wave Observatory, LIGO Document Control Center, California Institute of Technology, available at <http://admdbsrv.ligo.caltech.edu/dcc>
- Adhikari, R., González, G., Landry, M., & O’Reilly, B. 2003, *Class. Quantum Grav.*, 20, S903, iSI Document Delivery No.: 725RV Times Cited: 8 Sp. Iss. SI
- Barreiro, R. B., Hobson, M. P., Banday, A. J., Lasenby, A. N., Stolyarov, V., Vielva, P., & Górski, K. M. 2004, *MNRAS*, 351, 515
- Barreiro, R. B., Vielva, P., Hobson, M. P., Martínez-González, E., Lasenby, A. N., Sanz, J. L., & Toffolatti, L. 2001, in *Mining the Sky*, 465
- Barry, R. & Pace, R. K. 1999, *Linear Algebra and its Applications*, 289, 41
- Bennett, C. L., Hill, R. S., Hinshaw, G., Nolta, M. R., Odegard, N., Page, L., Spergel, D. N., Weiland, J. L., Wright, E. L., Halpern, M., Jarosik, N., Kogut, A., Limon, M., Meyer, S. S., Tucker, G. S., & Wollack, E. 2003, *ApJS*, 148, 97
- Burrows, A., & Hayes, J. 1996, *Physical Review Letters*, 76, 352
- Burrows, A., Livne, E., Dessart, L., Ott, C. D., & Murphy, J. 2006, *ApJL*, 640, 878
- . 2007, *ApJ*, 655, 416
- Dimmelmeier, H., Font, J. A., Müller, E. 2002, *A&A*, 393, 523

- Dimmelmeier, H., Ott, C. D., Janka, H.-T., Marek, A., & Müller, E. 2007, PRL submitted, astro-ph/0702305
- Evans, S. N. & Stark, P. B. 2002, *Inverse Problems*, 18, R55
- Ferrari, V., Miniutti, G., & Pons, J. A. 2003, *MNRAS*, 342, 629
- Finn, L. S. 1992, *Phys. Rev. D*, 46, 5236
- Finn, L. S. & Chernoff, D. F. 1993, *Phys. Rev. D*, 47, 2198
- Fryer, C. L., Holz, D. E., & Hughes, S. A. 2002, *ApJ*, 565, 430
- González, G., Landry, M., O’Reilly, B., & Radkins, H. 2004, Calibration of the LIGO detectors for S2, Tech. Rep. T040060-01-D, Laser Interferometer Gravitational Wave Observatory, LIGO Document Control Center, California Institute of Technology, available at <http://admdbsrv.ligo.caltech.edu/dcc>
- Gull, S. F. 1989, in *Maximum Entropy and Bayesian Methods*, ed. J. Skilling (Dordrecht: Kluwer Academic), 53–71
- Gull, S. F. & Daniell, G. J. 1978, *Nature*, 272, 686
- Gull, S. F. & Daniell, G. J. 1979, in *ASSL Vol. 76: IAU Colloq. 49: Image Formation from Coherence Functions in Astronomy*, 219
- Gürsel, Y. & Tinto, M. 1989, *Phys. Rev. D*, 40, 3884
- Heger, A., Langer, N., & Woosley, S. E. 2000, *ApJ*, 528, 368
- Heger, A., Woosley, S. E., Langer, N., & Spruit, H. C. 2004, in *IAU Symposium*, ed. A. Maeder & P. Eenens, 591–+
- Hobson, M. P. & Lasenby, A. N. 1998, *MNRAS*, 298, 905
- Jaynes, E. T. 1957a, *Phys. Rev.*, 106, 620
- . 1957b, *Phys. Rev.*, 108, 171
- Jones, A. W., Hancock, S., Lasenby, A. N., Davies, R. D., Gutierrez, C. M., Rocha, G., Watson, R. A., & Rebolo, R. 1998, *MNRAS*, 294, 582
- Jones, A. W., Lasenby, A. N., Mukherjee, P., Gutierrez, C. M., Davies, R. D., Watson, R. A., Hoyland, R., & Rebolo, R. 1999, *MNRAS*, 310, 105

- Lattimer, J. M. & Swesty, F. D. 1991, *Nucl. Phys A*, 535, 331
- Lazzarini, A. 2002, LIGO S1 Strain Sensitivity, Tech. Rep. G020461-01-E, Laser Interferometer Gravitational Wave Observatory, LIGO Document Control Center, California Institute of Technology, available at <http://admdbsrv.ligo.caltech.edu/dcc>
- . 2003, LIGO S2 Strain Sensitivity, Tech. Rep. G030379-00-E, Laser Interferometer Gravitational Wave Observatory, LIGO Document Control Center, California Institute of Technology, available at <http://admdbsrv.ligo.caltech.edu/dcc>
- . 2004, S3 Best Strain Sensitivities, Tech. Rep. G040023-00-E, Laser Interferometer Gravitational Wave Observatory, LIGO Document Control Center, California Institute of Technology, available at <http://admdbsrv.ligo.caltech.edu/dcc>
- . 2005, S4 Strain Sensitivities for the LIGO Interferometers, Tech. Rep. G050230-02-E, Laser Interferometer Gravitational Wave Observatory, LIGO Document Control Center, California Institute of Technology, available at <http://admdbsrv.ligo.caltech.edu/dcc>
- Lück, H. et al. 2006, *Class. Quantum Grav.*, 23, 71
- Mackay, D. J. C. 1992, *Neural Computation*, 4, 415
- Maisinger, K., Hobson, M. P., & Lasenby, A. N. 1997, *MNRAS*, 290, 313
- Maisinger, K., Hobson, M. P., & Lasenby, A. N. 2004, *MNRAS*, 347, 339
- Mandic, V. 2006, *PoS, HEP2005*, 037
- Misner, C. W., Thorne, K. S., & Wheeler, J. A. 1973, *Gravitation* (San Francisco: Freeman)
- Müller, E., Rampp, M., Buras, R., Janka, H.-T., & Shoemaker, D. H. 2004, *ApJ*, 603, 221
- Narayan, R. & Nityananda, R. 1986, *ARA&A*, 24, 127
- Nityananda, R. & Narayan, R. 1982, *Journal of Astrophysics and Astronomy*, 3, 419
- . 1983, *A&A*, 118, 194
- Ott, C. D., Burrows, A., Dessart, L., & Livne, E. 2006, *Phys. Rev. Lett.*, 96, 201102
- Ott, C. D., Burrows, A., Livne, E., & Walder, R. 2004, *ApJ*, 600, 834
- Ott, C. D., Dimmelmeier, H., Marek, A., Janka, H.-T., Zink, B., Hawke, I., & Schnetter, E. 2007, *CQG accepted*, astro-ph/0612638

- Pantin, E. & Starck, J.-L. 1996, *Astron. Astrophys. Supp.*, 118, 575
- Ponsonby, J. E. B. 1973, *MNRAS*, 163, 369
- Rakhmanov, M. 2006, *Class. Quantum Grav.*, S673
- Rampp, M., Mueller, E., & Ruffert, M. 1998, *A&A*, 332, 969
- Robertson, N. A. 2000, *Class. Quantum Grav.*, 17, 19
- Rüdiger, A. 2004, in *Observing, Thinking and Mining the Universe*, 329–+
- Shevgaonkar, R. K. 1987, *A&A*, 176, 159
- Shibata, M., & Sekiguchi, Y.-I. 2005, *Phys. Rev. D*, 71, 024014
- Skilling, J. & Bryan, R. K. 1984, *MNRAS*, 211, 111
- Starck, J. & Pantin, E. 1996, *Vistas in Astronomy*, 40, 563
- Starck, J. & Pantin, E. 1997, in *Statistical Challenges in Modern Astronomy II*, 405
- Steenstrup, S. 1985, *Australian Journal of Physics*, 38, 319
- Takahashi, R. & the TAMA Collaboration. 2004, *Class. Quantum Grav.*, 21, S403
- Vielva, P., Barreiro, R. B., Hobson, M. P., Martínez-González, E., Lasenby, A. N., Sanz, J. L., & Toffolatti, L. 2001, *MNRAS*, 328, 1
- Waldman, S. J. & the LIGO Science Collaboration . 2006, *Class. Quantum Grav.*, 23, S653
- Woosley, S. E. & Weaver, T. A. 1995, *ApJS*, 101
- Woosley, S. E., & Bloom, J. S. 2006, *ARA&A*, 44, 507

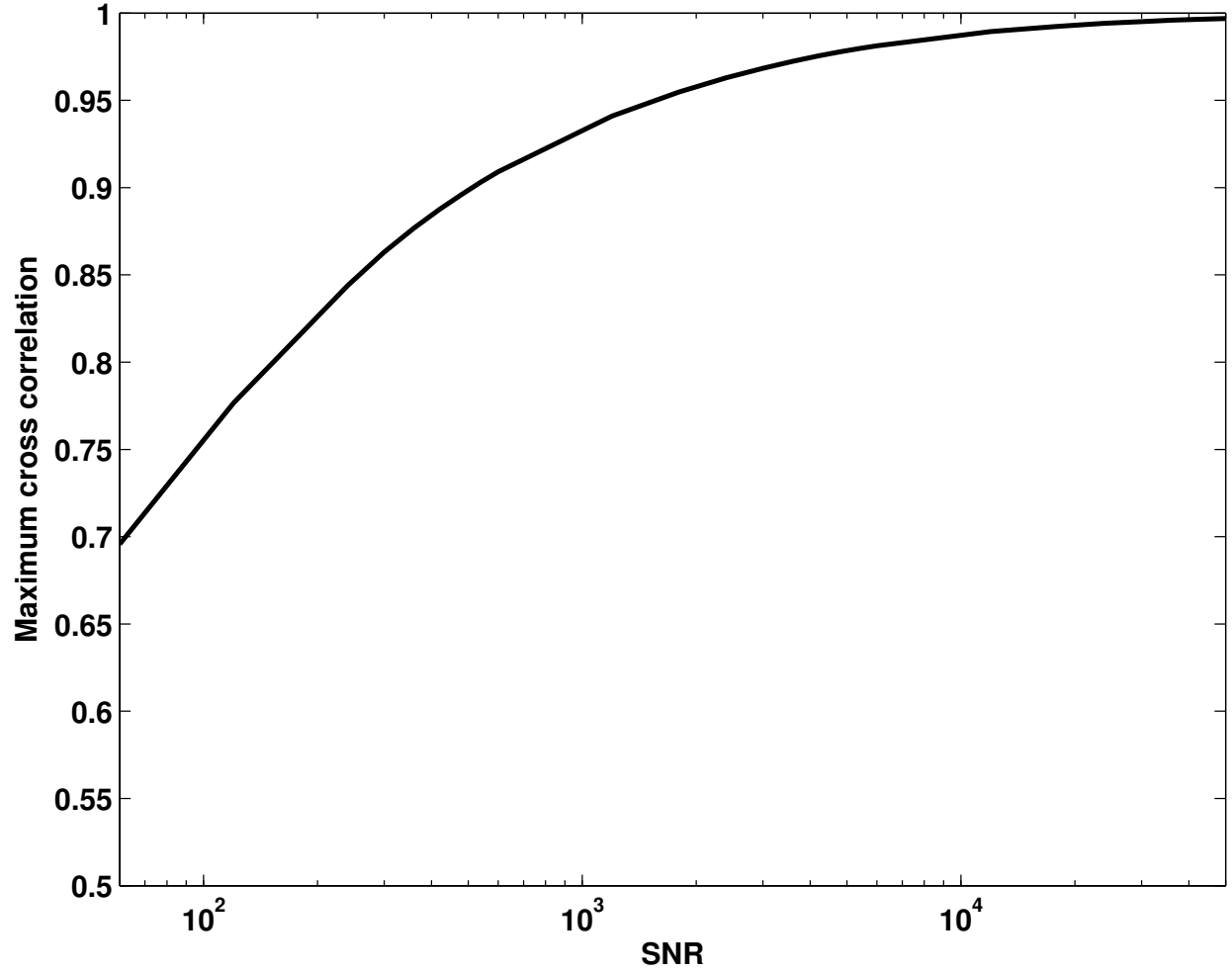


Fig. 1.— Maximum cross-correlation between the inferred and initial core collapse signal at different ρ^2 using maximum entropy.

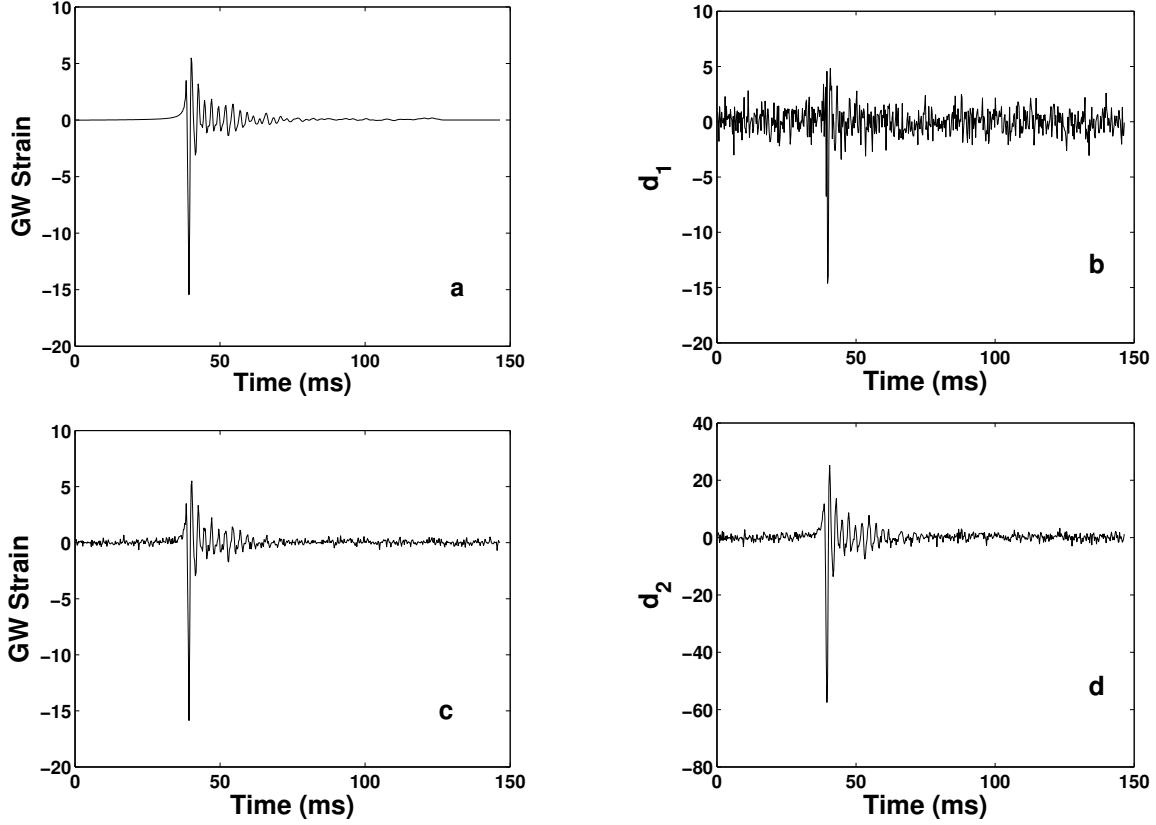


Fig. 2.— Estimation of core collapse signal for high $\rho^2 = 6000$. (a) Portion of waveform (Ott et al. (2004) s15A1000B0.1) used as initial signal. The waveform is scaled to correspond to a core collapse event at 10 kpc. (b) Data stream \mathbf{d}_1 formed by convolving the initial signal with the simple filter $[1 \ -2 \ 2]$ and adding white, Gaussian noise. (c) Maximum entropy estimated signal. (d) Data stream \mathbf{d}_2 formed by convolving the initial signal with the simple filter $[1 \ 2 \ 2]$ and adding white, Gaussian noise. The convolved signal created using the filter $[1 \ 2 \ 2]$ has a higher amplitude than the signal created with $[1 \ -2 \ 2]$. The amplitude of the noise is chosen so that the average ρ^2 for the two, convolved signals is 6000 and the same amplitude noise is added to both signals. Maximum entropy does a good job of estimating the initial signal.

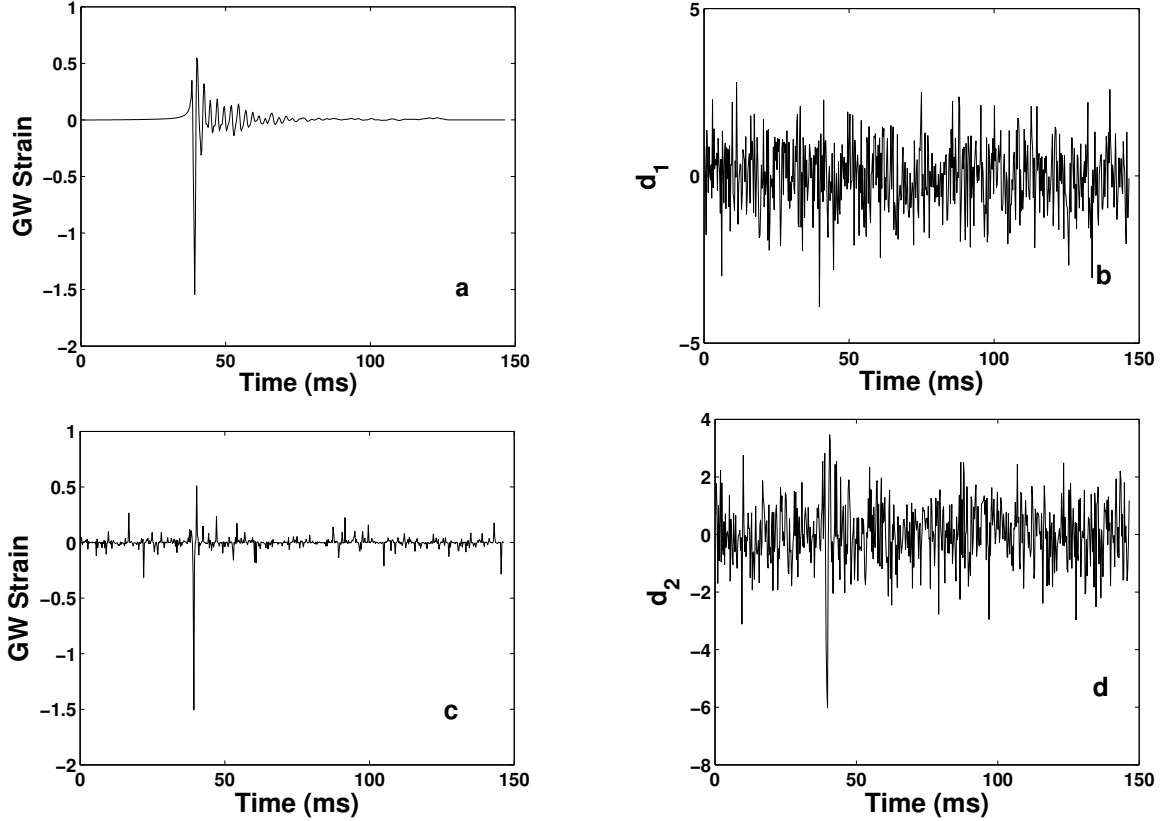


Fig. 3.— Estimation of core collapse signal for low $\rho^2 = 60$. (a) Portion of waveform (Ott et al. (2004) s15A1000B0.1) used as initial signal. The waveform is scaled to correspond to a core collapse event at 10 kpc. This model emits a total energy of $\sim 6.6 \times 10^{-9} M_{\odot} c^2$ in gravitational waves, of which $\sim 90\%$ are emitted in the pronounced spike associated with core bounce. (b) Data stream \mathbf{d}_1 formed by convolving the initial signal with the simple filter $[1 \ -2 \ 2]$ and adding white, Gaussian noise. (c) Maximum entropy estimated signal. (d) Data stream \mathbf{d}_2 formed by convolving the initial signal with the simple filter $[1 \ 2 \ 2]$ and adding white, Gaussian noise. The convolved signal created using the filter $[1 \ 2 \ 2]$ has a higher amplitude than the signal created with $[1 \ -2 \ 2]$. The amplitude of the noise is chosen so that the average ρ^2 for the two, convolved signals is 60 and the same amplitude noise is added to both signals. Maximum entropy does a fair job of estimating the signal

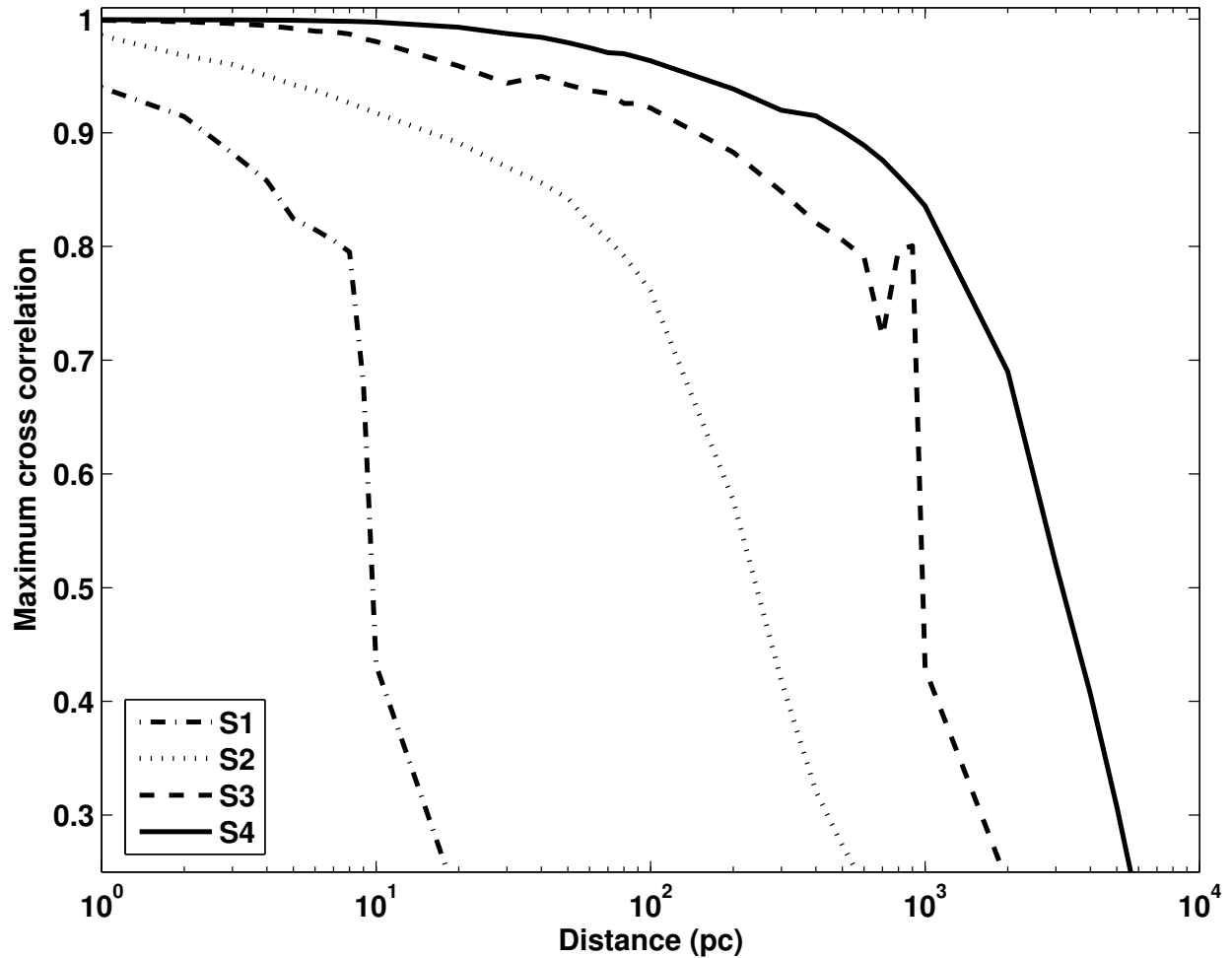


Fig. 4.— Maximum cross-correlation between estimated and initial signals versus core collapse distance for data simulated using different science run detector impulse responses and noise levels. The estimated signal is inferred using maximum entropy from simulated detections that use Ott et al. (2004) model s15A1000B0.1 as the initial signal waveform. The up-tick in the S3 run, located at approximately 1 kpc, is the result of a discontinuous change in the most probable waveform. There is a steady improvement in maximum entropy’s ability to reconstruct fainter, more distant signals as the sensitivity of the detectors improved (Lazzarini 2002, 2003, 2004, 2005).

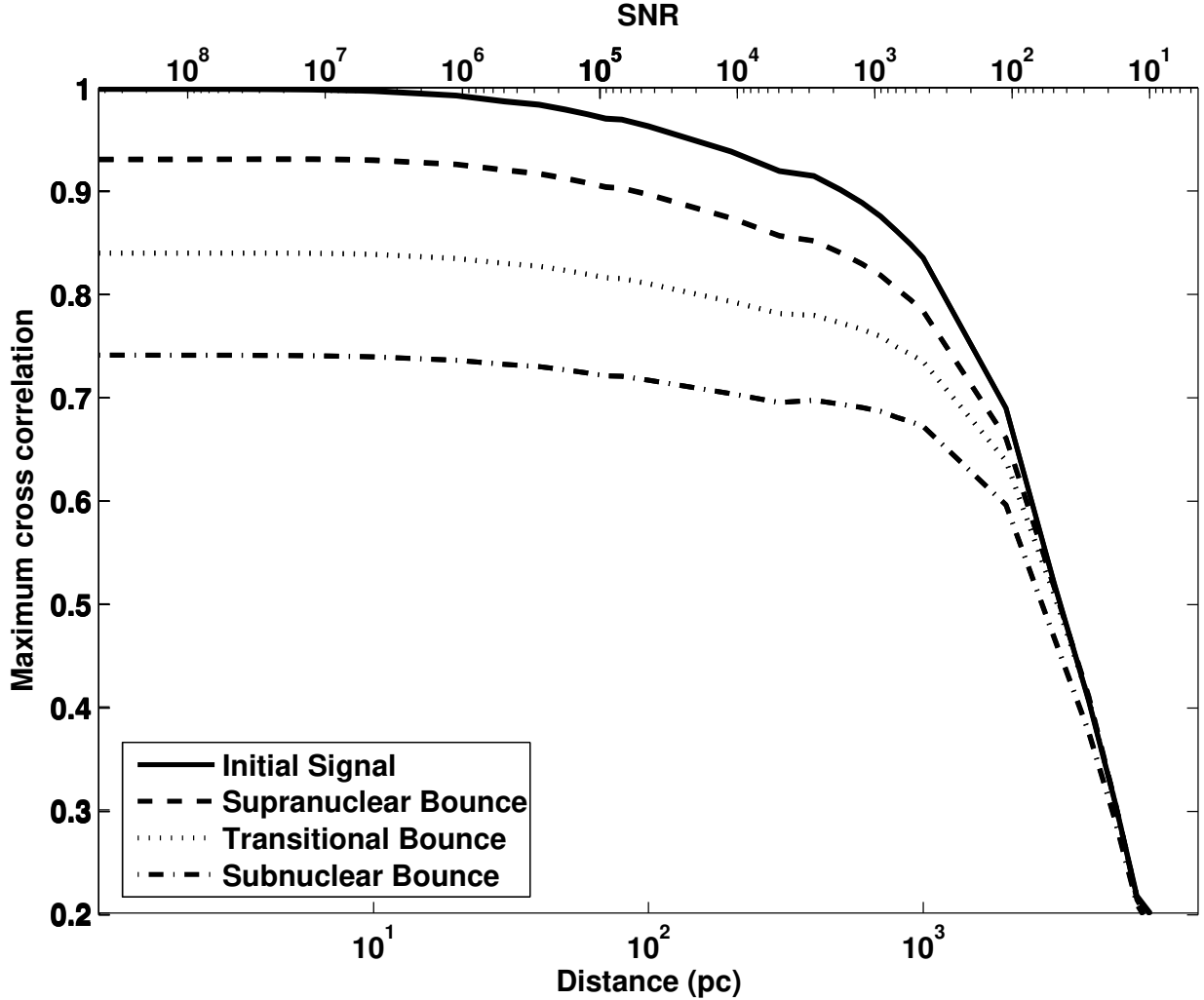


Fig. 5.— Maximum cross-correlation between reconstructed waveforms and waveforms associated with models that differ by bounce type versus core collapse distance and ρ^2 . The ρ^2 shown is the average for the two detectors. The ρ^2 for the 4-km Hanford detector is 1.05 times that shown while the ρ^2 for the 4-km Livingston detector is 0.95 times that shown. The reconstructed waveform is inferred using maximum entropy from simulated detections that use the waveform from the Ott et al. (2004) model s15A1000B0.1 as the initial signal waveform as well as detector responses and noise levels from the fourth science run (S4). The solid line represents the maximum cross-correlation between the reconstructed signal and the initial signal waveform. The other lines represent the maximum cross-correlations between the inferred waveforms and the waveforms resulting from each bounce type for which the maximum cross-correlation at 1 pc is greatest, excluding that used for the initial signal. The inferred waveform is most similar to those generated by models with the same, supranuclear bounce type as the initial signal waveform, for the simulations corresponding to core collapse events that occur less than 2-3 kpc away.

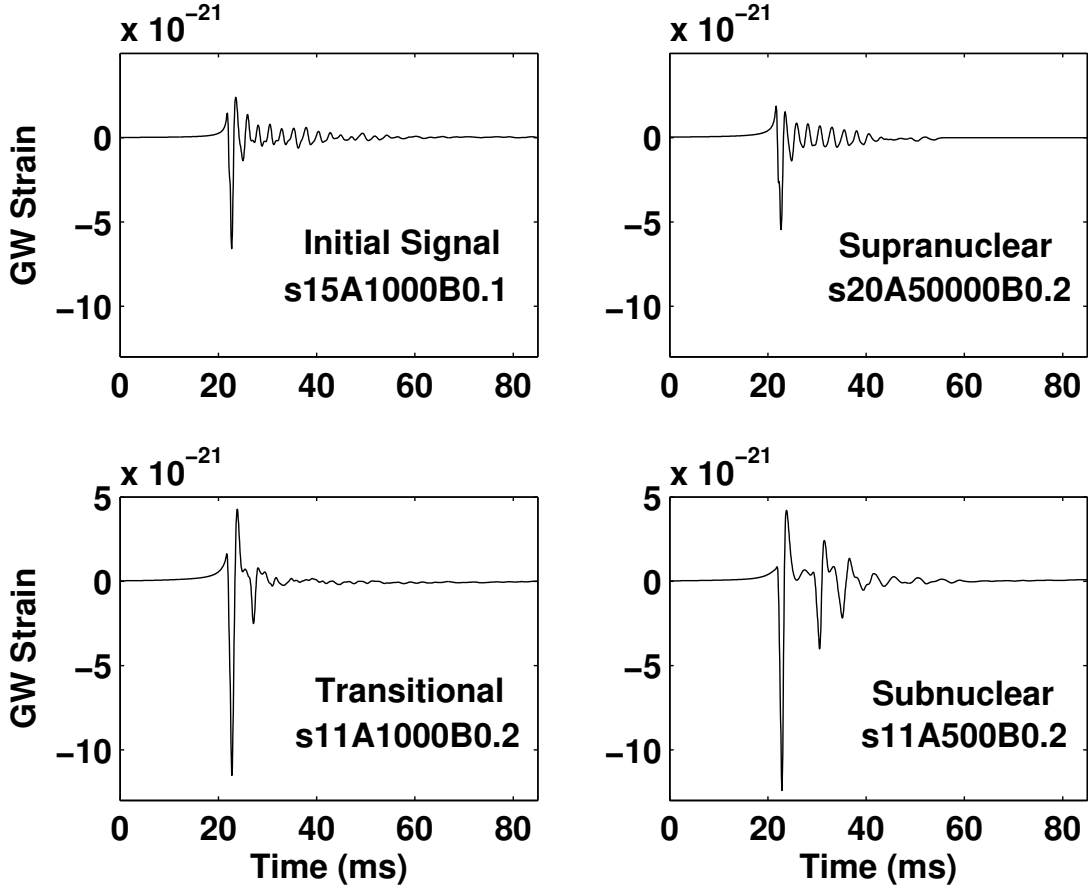


Fig. 6.— The waveforms associated with various bounce types that are compared with the inferred signal in Fig. 5. The upper left plot shows the waveform (from Ott et al. [2004] model s15A1000B0.1) that was used as the initial signal in the simulated detection. The three other waveforms shown are those that are most similar to this initial signal waveform, for each bounce type. The waveform from the Ott et al. (2004) s20A50000B0.2 model looks much like the initial signal waveform which is of the same, supranuclear bounce type. The subnuclear bounce waveform shows the effects of multiple damped, harmonic oscillator-like expansion-collapse-bounce cycles. The zero points of the time axes are chosen so that the minima of the waveforms occur at the same time for ease of comparison. The waveform amplitudes are scaled to correspond to core collapse events at 10 kpc.

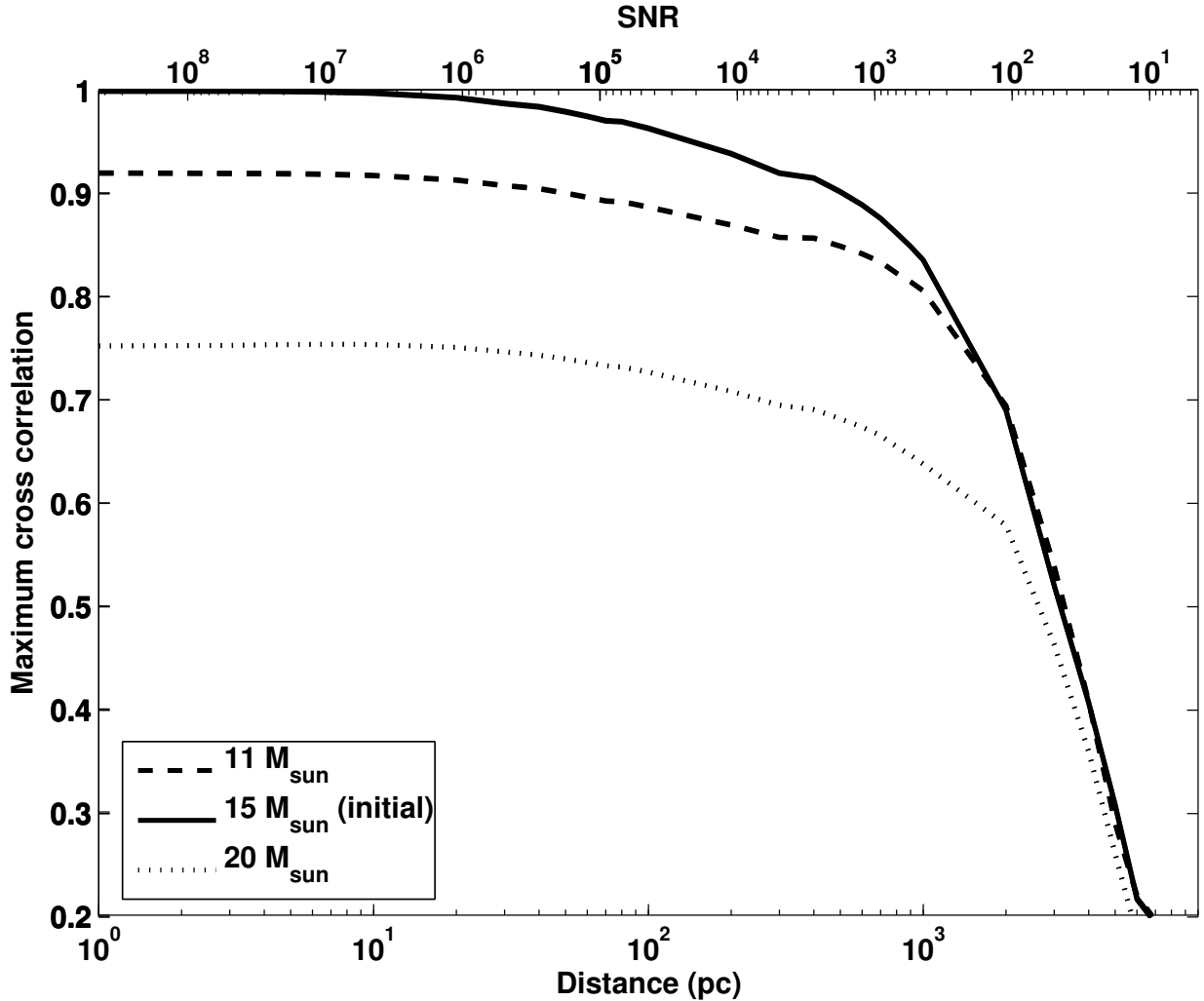


Fig. 7.— Maximum cross-correlation between reconstructed waveforms and waveforms associated with models that differ only by progenitor mass versus core collapse distance and ρ^2 . The ρ^2 shown is the average for the two detectors. The ρ^2 for the 4-km Hanford detector is 1.05 times that shown while the ρ^2 for the 4-km Livingston detector is 0.95 times that shown. The reconstructed waveform is inferred using maximum entropy from simulated detections that use a waveform from a model with a progenitor mass of 15 solar masses (Ott et al. [2004] model s15A1000B0.1) as the initial signal waveform as well as detector responses and noise levels from the fourth science run (S4). The inferred waveform is most similar to that generated by the model with the same progenitor mass for the simulations corresponding to core collapse events that occur less than 2-3 kpc away.

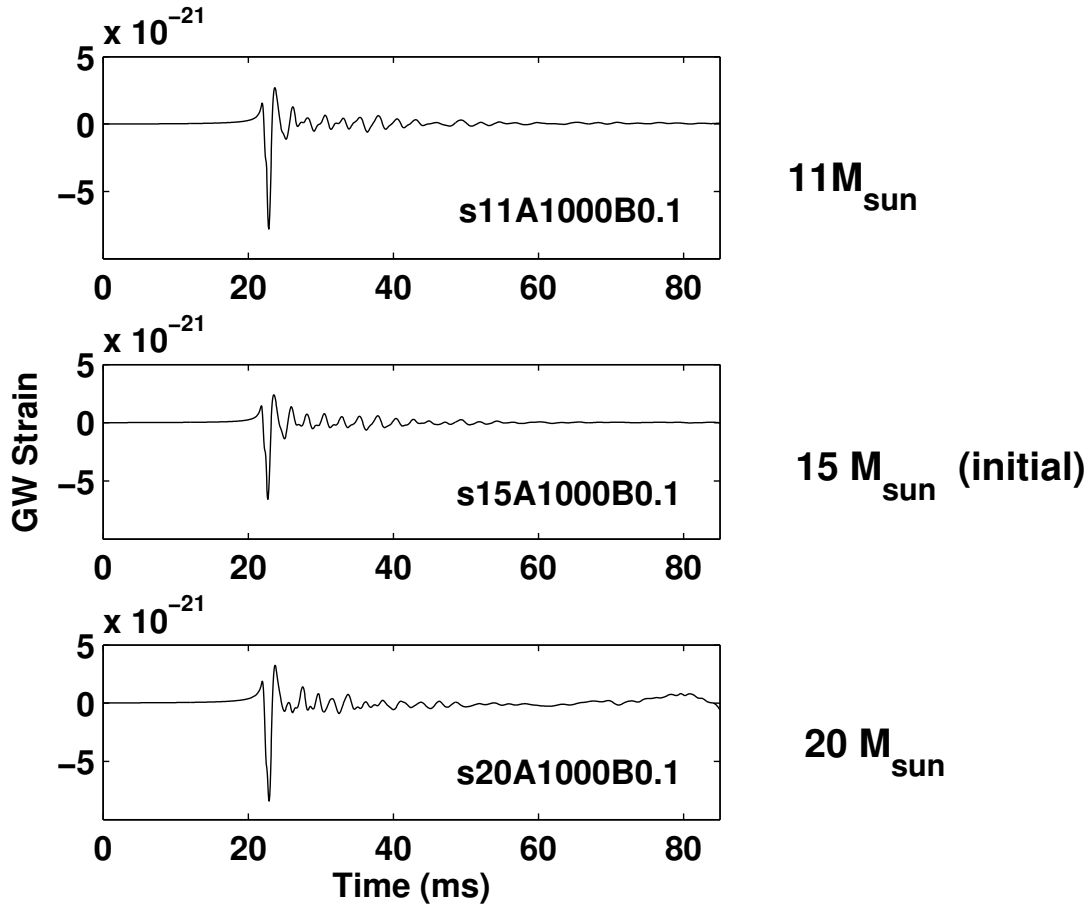


Fig. 8.— Waveforms from models that differ only by progenitor mass. The waveform corresponding to Ott et al. (2004) model s15A1000B0.1 was used as the initial signal in the detection simulations. The zero points of the time axes are chosen so that the minima of the waveforms occur at the same time for ease of comparison. The waveform amplitudes are scaled to correspond to core collapse events at 10 kpc.

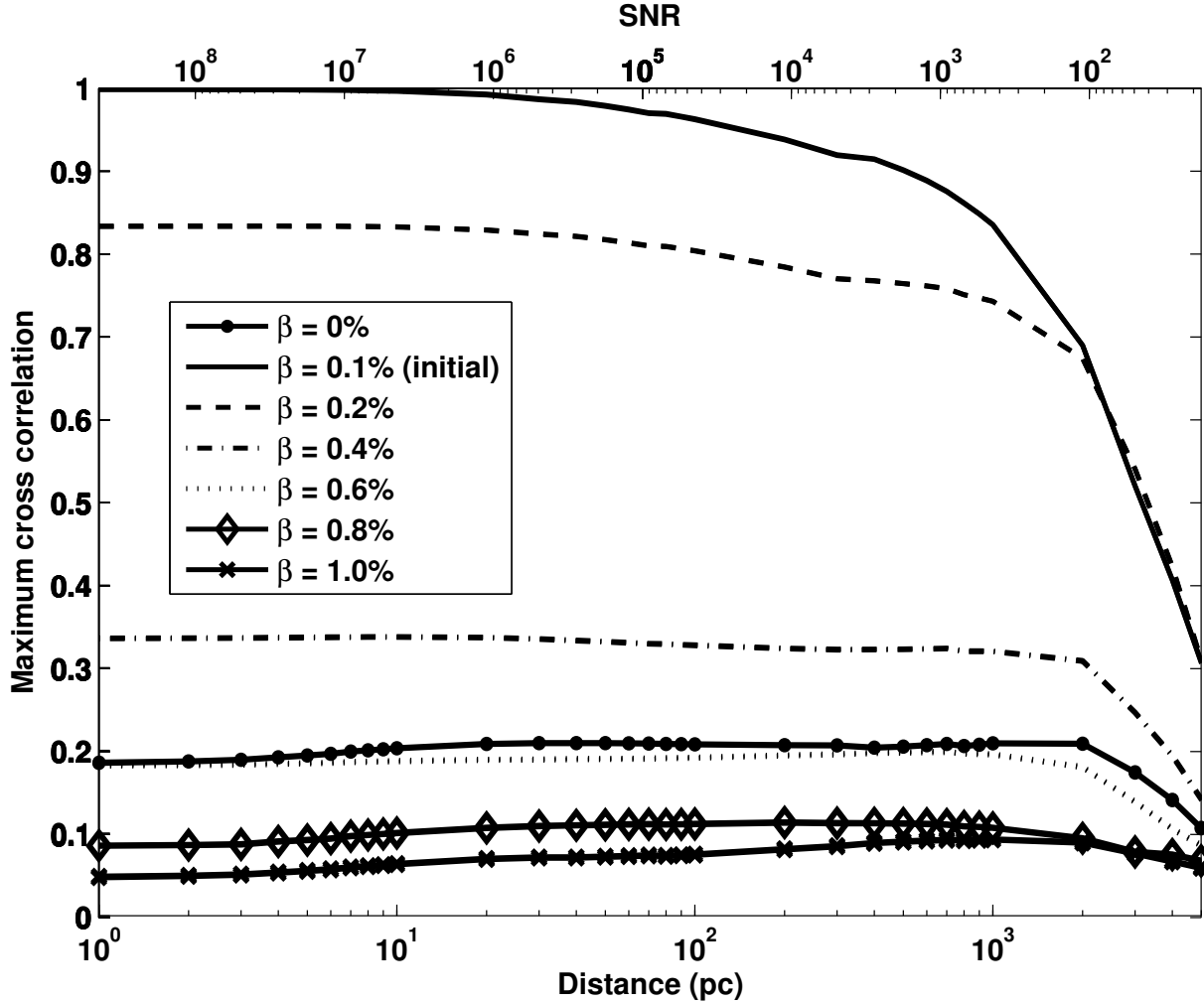


Fig. 9.— Maximum cross-correlation between reconstructed waveforms and waveforms associated with models that differ only by rotation parameter β , which is defined in equation (25), versus core collapse distance and ρ^2 . The ρ^2 shown is the average for the two detectors. The ρ^2 for the 4-km Hanford detector is 1.05 times that shown while the ρ^2 for the 4-km Livingston detector is 0.95 times that shown. The reconstructed waveform is inferred using maximum entropy from simulated detections that use a waveform from a model with a rotation parameter of $\beta = 0.1\%$ (Ott et al. [2004] model s15A1000B0.1) as the initial signal waveform as well as detector responses and noise levels from the fourth science run (S4). The inferred waveform is most similar to that generated by the model with the same β for the simulations corresponding to core collapse events that occur less than 2-3 kpc away.

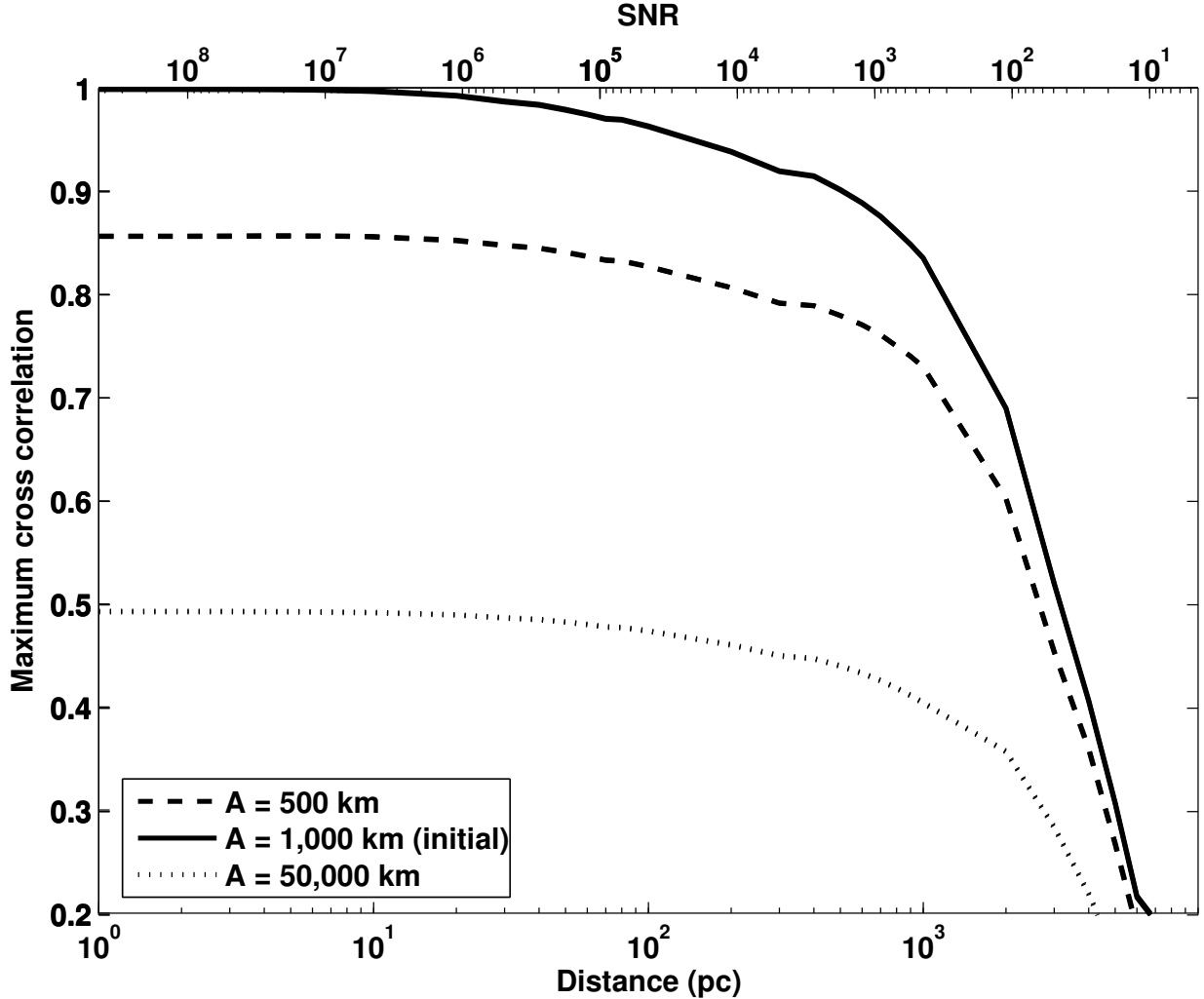


Fig. 10.— Maximum cross-correlation between reconstructed waveforms and waveforms associated with models that differ only by initial degree of differential rotation as parameterized by A , which is defined in equation (26), versus core collapse distance and ρ^2 . The ρ^2 shown is the average for the two detectors. The ρ^2 for the 4-km Hanford detector is 1.05 times that shown while the ρ^2 for the 4-km Livingston detector is 0.95 times that shown. The reconstructed waveform is inferred using maximum entropy from simulated detections that use a waveform from a model with a differential rotation parameter of $A = 1,000$ km (Ott et al. [2004] model s15A1000B0.1) as the initial signal waveform as well as detector responses and noise levels from the fourth science run (S4). The inferred waveform is the most similar to that generated by the model with the same initial degree of differential rotation.

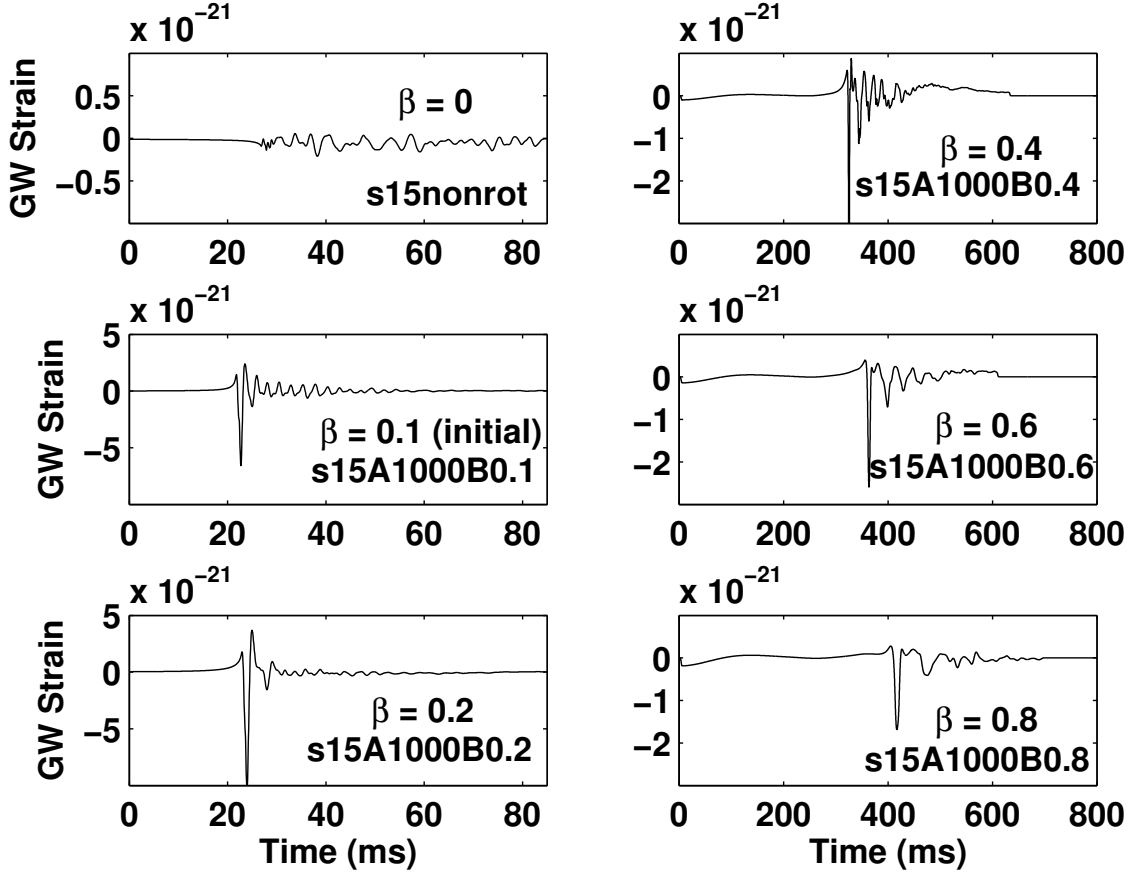


Fig. 11.— Waveforms from models that differ only by rotation parameter β , defined by equation (25). The waveforms for larger β ($\geq 0.4\%$) have significant amplitude over durations of hundreds of ms, while low β waveforms last only for tens of ms. The $\beta = 0\%$ waveform has very low amplitude as the non-rotating collapse is nearly spherically symmetric. The waveform corresponding to Ott et al. (2004) model s15A1000B0.1 was used as the initial signal in the detection simulations. The zero point of the time axes for the plots on the right is chosen so that the onset of significant gravitational wave amplitude occurs at roughly the same time while the plots on the left show the first 800 ms of the waveform. The waveform amplitudes are scaled to correspond to core collapse events at 10 kpc.

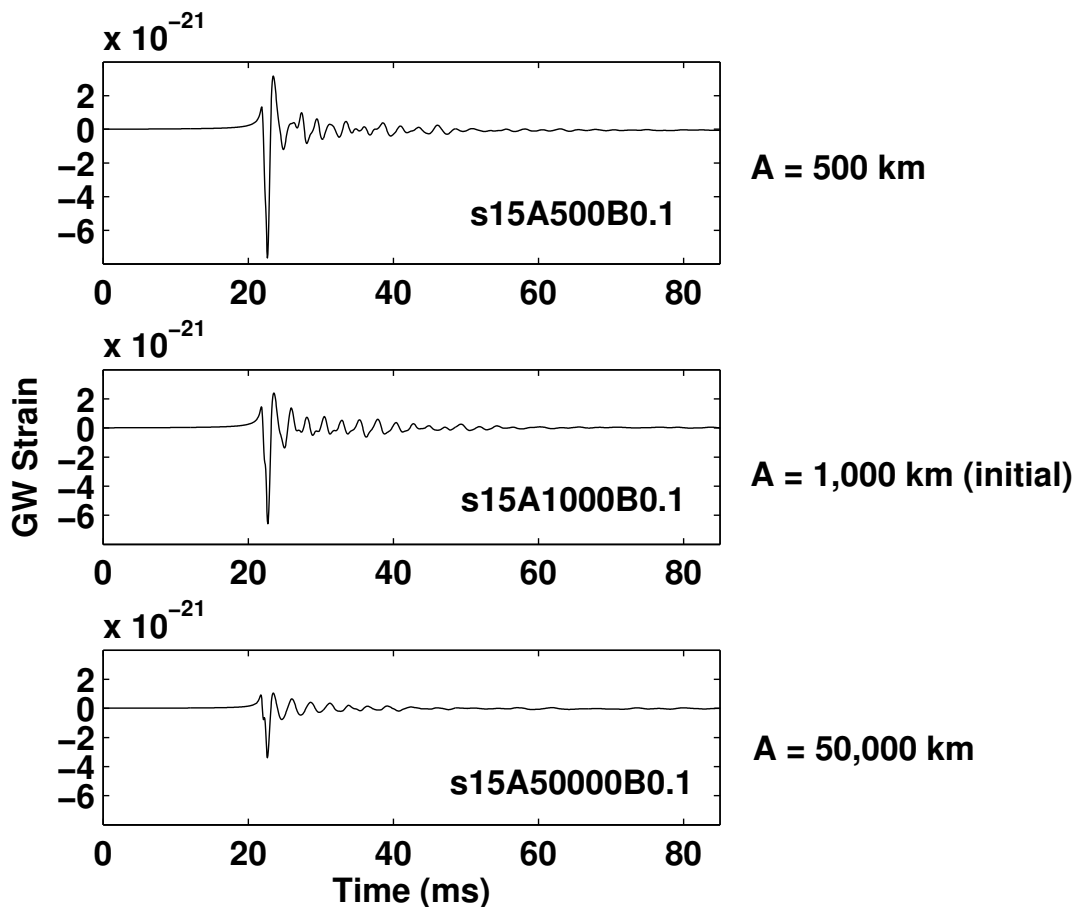


Fig. 12.— Waveforms from models that differ only by initial degree of differential rotation. The differential rotation parameter, A , is the distance at which the rotational velocity of the progenitor drops to half the rotational velocity at its center. As A decreases the differential rotation of the progenitor becomes more extreme and the amplitudes of the gravitational waves increase. The center plot shows the waveform corresponding to Ott et al. (2004) model $s15A1000B0.1$ which was used as the initial signal in the detection simulations. The zero points of the time axes are chosen so that the minima of the waveforms occur at the same time for ease of comparison. The waveform amplitudes are scaled to correspond to core collapse events at 10 kpc.